

A Simulation Study of the Mesoscale Convective Systems Associated with a Meiyu Frontal Heavy Rain Event*

ZHANG Jin (张进) and TAN Zhemin[†] (谈哲敏)

Key Laboratory of Mesoscale Severe Weather/MOE, and School of Atmospheric Sciences, Nanjing University, Nanjing 210093

(Received January 20, 2009; revised February 25, 2009)

ABSTRACT

In this study, evolution of the mesoscale convective systems (MCSs) within a Meiyu front during a particularly heavy rainfall event on 22 June 1999 in East China was simulated by using a nonhydrostatic numerical model ARPS (Advanced Regional Prediction System). Investigations were conducted with emphasis on the impact of the interaction among multi-scale weather systems (MWSs) on the development of MCSs in the Meiyu frontal environment.

For this case, the development of MCSs experienced three different stages. (1) The convections associated with MCSs were firstly triggered by the eastward-moving Southwest Vortex (SWV) from the Sichuan Basin, accompanying the intensification of the upper-level jet (ULJ) and the low-level jet (LLJ) that were approaching the Meiyu front. (2) Next, a low-level shear line (LSL) formed, which strengthened and organized the MCSs after the SWV decayed. Meanwhile, the ULJ and LLJ enhanced and produced favorable conditions for the MCSs development. (3) Finally, as the MCSs got intensified, a mesoscale convective vortex (MCV), a mesoscale LLJ and a mesoscale ULJ were established. Then a coupled-development of MWSs was achieved through the vertical frontal circulations, which further enhanced the MCV and resulted in the heavy rainfall. This is a new physical mechanism for the formation of Meiyu heavy rainfall related to the SWV during the warm season in East China.

In the three stages of the heavy rainfall, the vertical frontal circulations exhibited distinguished structures and played a dynamic role, and they enhanced the interaction among the MWSs. A further examination on the formation and evolution of the MCV showed that the MCV was mainly caused by the latent heat release of the MCSs, and the positive feedback between the MCSs and MCV was a key characteristic of the scale interaction in this case.

Key words: mesoscale convective systems (MCSs), mesoscale convective vortex (MCV), scale interaction, Meiyu front

Citation: Zhang Jin and Tan Zhemin, 2009: A simulation study of the mesoscale convective systems associated with a Meiyu frontal heavy rain event. *Acta Meteor. Sinica*, **23**(4), 438–454.

1. Introduction

The Meiyu (also called Baiu in Japan and Changma in Korea) front, a quasi-stationary or slow-moving frontal system, is one of the most important weather systems that dominate the warm season over East Asia, especially in the middle and lower reaches of the Yangtze River (hereafter MLYR) of China. The mature structure of the Meiyu front is characterized by a weak horizontal temperature gradient, but a strong horizontal moisture contrast (Ding, 1992).

Usually, a low-level shear line (LSL), which possesses strong cyclonic vorticity due to horizontal wind shear in the lower troposphere, accompanies the Meiyu front (e.g., Akiyama, 1973; Kato, 1985). The Meiyu frontal heavy rainfall responsible for flooding disasters over the MLYR in warm seasons is directly caused by the mesoscale convective systems (MCSs) which usually form, propagate, and organize along the front (Chen et al., 1998). There also exist other weather systems on different scales which contribute to the Meiyu precipitation, such as the low-level mesoscale vortex (LMV)

*Supported by the State Key Basic Research Program (2004CB18300), the National Natural Science Foundation of China under Grant Nos. 40828005, 40325014, and 40333031, DPHE (20080284019), the Key Project of Ministry of Education of China (No. 02109), and the National Special Funding Project for Meteorology (GYHY200706033).

[†]Corresponding author: zmtan@nju.edu.cn.

(including the southwest vortex (SWV), the mesoscale convective vortex (MCV), etc.), the low-level jet (LLJ), and the upper-level jet (ULJ) within the Meiyu front. It has been demonstrated that the interaction among these multi-scale weather systems (hereafter MWSs) at both lower and upper levels has a profound impact on the evolution and organization of the MCSs embedded in the Meiyu front, as well as the amount and distribution of the heavy rainfall (Liao and Tan, 2005). However, such a scale interaction is nonlinear and highly complicated, so studies in this regard are far from definitive at present.

Previous studies found that the SWV, which is one kind of LMV generated near the eastern foothill of the Tibetan Plateau, usually migrates eastward to the coast of China and causes heavy rainfall along its path (Kuo et al., 1986, 1988). When it arrives in the Yangtze and Huaihe River basins (hereafter YHRB), the SWV often develops into a strong mesoscale cyclone known as the Yangtze-Huaihe cyclone, and vibrantly interacts with the MCSs and leads to localized heavy rainfalls. Gao and Xu (2001) found that an SWV along the Meiyu front on 22 June 1999 experienced a process of demise in the upstream and revival in the downstream (i.e., jumping-shift) when it propagated eastward, and then brought a heavy rainfall in the YHRB, but how exactly the jumping-shift process operated and geared was not disclosed in that study. Besides the SWV, there often exists another kind of LMV along the Meiyu front. It often emerges under favorable thermodynamic and dynamic conditions, and is closely connected with the LSL and the LLJ (Hu and Pan, 1996). This kind of LMV frequently triggers and/or enhances the MCSs along the Meiyu front. In terms of vorticity, this kind of LMV is similar to the SWV, and is sometimes incorrectly regarded as the SWV. In the present study, different from the SWV jumping-shift mechanism in Gao and Xu (2001), a new mechanism for the formation of Meiyu heavy rain under the scale interaction among the various MWSs is proposed.

Regarding the ULJ and LLJ that often accompany Meiyu fronts, earlier studies have shown that they play an indispensable role in the development of

MCSs and formation of Meiyu precipitation. A well-defined synoptic-scale LLJ usually occurs to the south of a Meiyu front, which transports warm and moist air northward, and creates a convectively unstable layer favorable for the development of MCSs (Chen, 1983). The divergence near the rear-right quadrant of the ULJ streak, a favorable position relative to the low-level Meiyu front, can induce additional uplifting that supports the enhancement of MCSs and the Meiyu front (Chen et al., 2003). It is noted that a mesoscale LLJ (mLLJ) and a mesoscale ULJ (mULJ) are often located, respectively, to the south and east of a mature MCS embedded in the Meiyu front (Chen et al., 2000). Here, we refer to mLLJ/mULJ as a jet core of LLJ/ULJ along the Meiyu front, with an obvious maximum wind speed and a horizontal scale of a few hundred kilometers. Based on numerical simulations, Chen et al. (2000) concluded that the mLLJ/mULJ forms in response to intense convections associated with MCSs. The mLLJ injects more warm and moist air into the MCS through strong low-level convergence on its left front. Much of inflow into the MCS extends up to the upper troposphere and ventilates through the mULJ, which enhances the upper-level divergence immediately near the MCS.

Although significant progress in understanding Meiyu heavy rainfalls have been achieved in previous studies, the scale interaction within the Meiyu front and its effect on the MCSs and associated precipitation remain not studied so far. Accurate quantitative forecast of the Meiyu heavy rainfall is still a difficult task (e.g., Yang et al., 2004; Chu et al., 2007). In this paper, we focus on the understanding of how the scale interaction operates and impacts the development of the MCSs along the Meiyu front based on a numerical simulation of a Meiyu frontal heavy rain event that occurred on 22 June 1999.

The rest of this paper is organized as follows: A brief synoptic overview is presented in Section 2. Section 3 provides a model description as well as an assessment of the model simulation. The scale interaction among the MWSs and its impact on the MCSs are analyzed in Section 4. A detailed analysis on the development mechanisms of MCV and its interaction

with the MCSs are presented in Section 5. Conclusions and discussion are given in Section 6.

2. Synoptic overview

2.1 Observed rainfall and the MCSs

A particular heavy rainfall event occurred on 22 June 1999 over the MLYR. The observed 24-h accumulated rainfall ending at 0000 UTC 23 June 1999 was distributed southwest-northeast along the MLYR, with four high precipitation centers (Fig. 1a). There are 71 stations with recorded rainfall exceeding 50 mm and 10 stations beyond 100 mm.

The heavy rainfall was resulted from a succession of MCSs, which developed from scattered cloud clusters to an organized cloud band along the Meiyu front in the 24-h period. Infrared (IR) images from the Japanese Geostationary Meteorological Satellite (GMS) at a 3-h interval were used to illustrate the temporal evolution of the MCSs along the MLYR (Fig. 2). From 0000 UTC to 0900 UTC 22 June, there was an obvious MCS located over the middle reaches of the Yangtze River (Figs. 2a-d). In the next 6 h, a mesoscale convective cloud band, embedded evidently in some convective systems, formed in the middle reaches of the Yangtze River, and it extended to the YHRB (Figs. 2e, 2f). Up till 1800 UTC 22 June,

an organized cloud band, about 2000-km long and constituted mainly of a series of active MCSs, formed along the MLYR (Fig. 2g). In the next 6 h, the convective cloud band was remarkably strengthened along the MLYR (Figs. 2h, 2i). The associated MCSs became mature with expanded size and enhanced intensity.

2.2 Synoptic situation and the Meiyu front

At 0000 UTC 22 June 1999, a planetary-scale westerly belt at 300 hPa was located to the north of the MLYR. A ULJ streak with a maximum westerly wind speed of about 50 m s^{-1} was found nearby (40°N , 115°E) (Fig. 3a). In the following 24 h, the ULJ streak strengthened and extended to the northeast. By 0000 UTC 23 June, the ULJ streak was dominated by southwesterly wind, with its rear-right quadrant located over the YHRB (Fig. 3b).

At 500 hPa, the western segment of the western Pacific subtropical high (WPSH) ridge extended to 15°N , 120°E at 0000 UTC 22 June, with a strong warm and moist southwesterly flow appearing to its west and northwest (Fig. 3c). In middle latitudes, a trough was located from northeastern China to the YHRB. Meanwhile, there were two other shortwave troughs, located over the middle reaches of the Yellow River and the eastern Yungui Plateau, respectively.

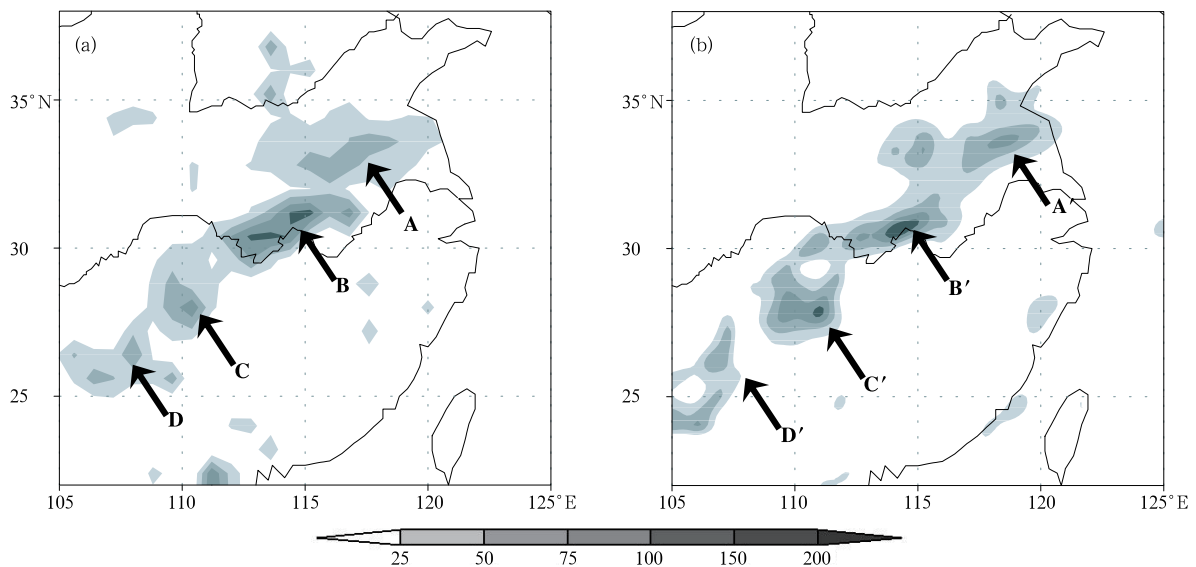


Fig. 1. Observed (a) and simulated (b) 24-h accumulated rainfall (shaded; mm) from 0000 UTC 22 to 0000 UTC 23 June 1999.

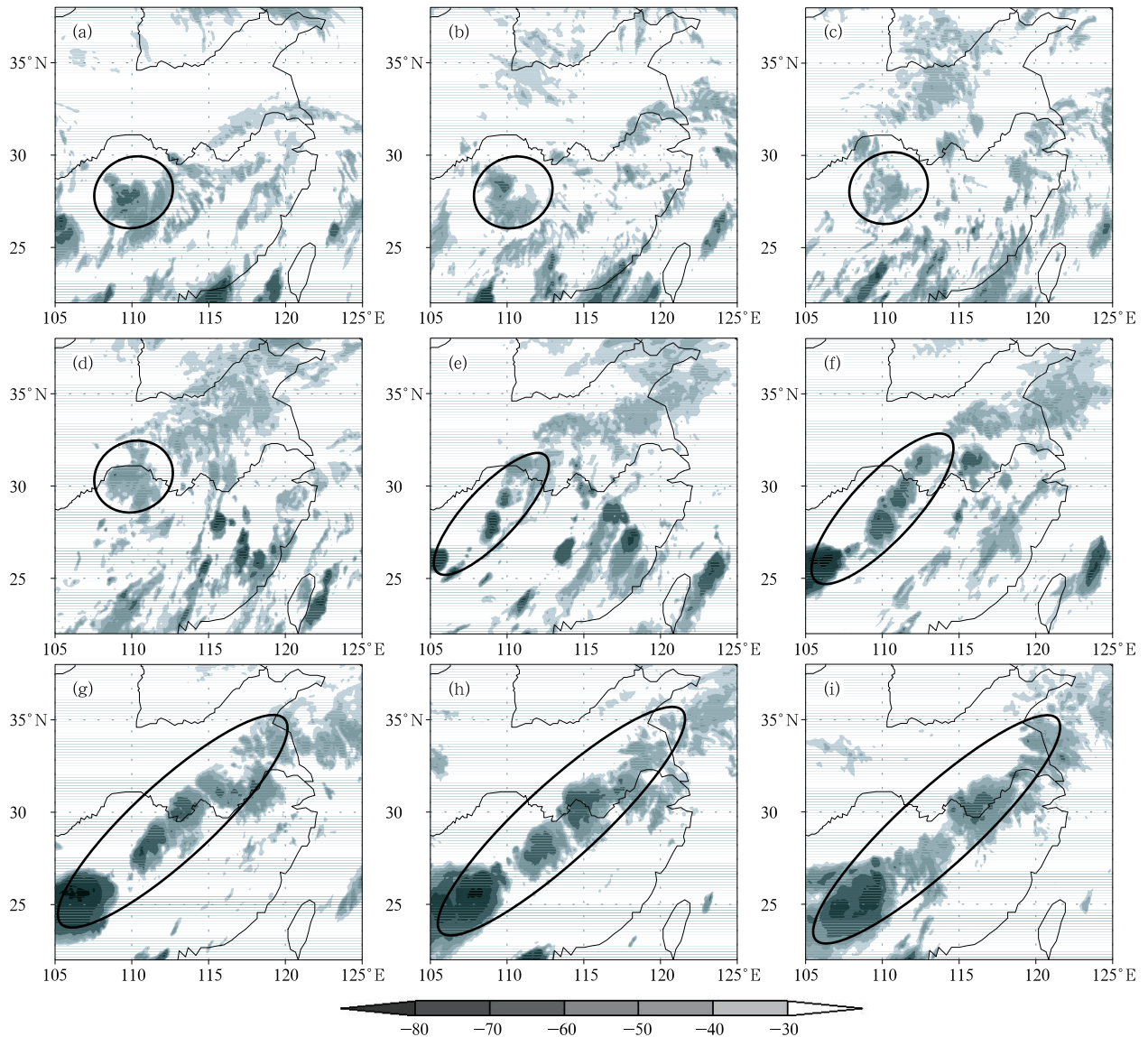


Fig. 2. The satellite brightness temperature (shaded; °C) valid between 0000 UTC 22 and 0000 UTC 23 June 1999 at an interval of 3 h.

At 0000 UTC 23 June, the WPSH was intensified and the southwesterly flow along its northwestern side was also accelerated (Fig. 3d). Over the MLYR, the trough over northeastern China merged with the shortwave trough over the Yungui Plateau. A major trough running through mainland China came into play. The cold air flow behind the trough strengthened and encountered the warm and moist southwesterly flow over the MLYR, leading to a favorable synoptic environment for the Meiyu frontogenesis.

At 850 hPa, an SWV at a horizontal scale of 500 km maintained over the Sichuan Basin, with its center

located at 30°N, 105°E at 0000 UTC 22 June (Fig. 3e). Besides, a short LSL was over the YHRB, with southwesterly flows to the south and a large stretch of southeasterly flows to the north. But this LSL died away as the southwesterly accelerated northward in the following 6 h, and had little impact on the rainfall. Up to 0000 UTC 23 June, a new well-defined LSL, with an LMV located at its northeastern end, formed over the MLYR with intensified southwesterly flows to the south and strong northeasterly flows to the north (Fig. 3f). The enhancement of the cyclonic flow promoted the Meiyu frontogenesis through

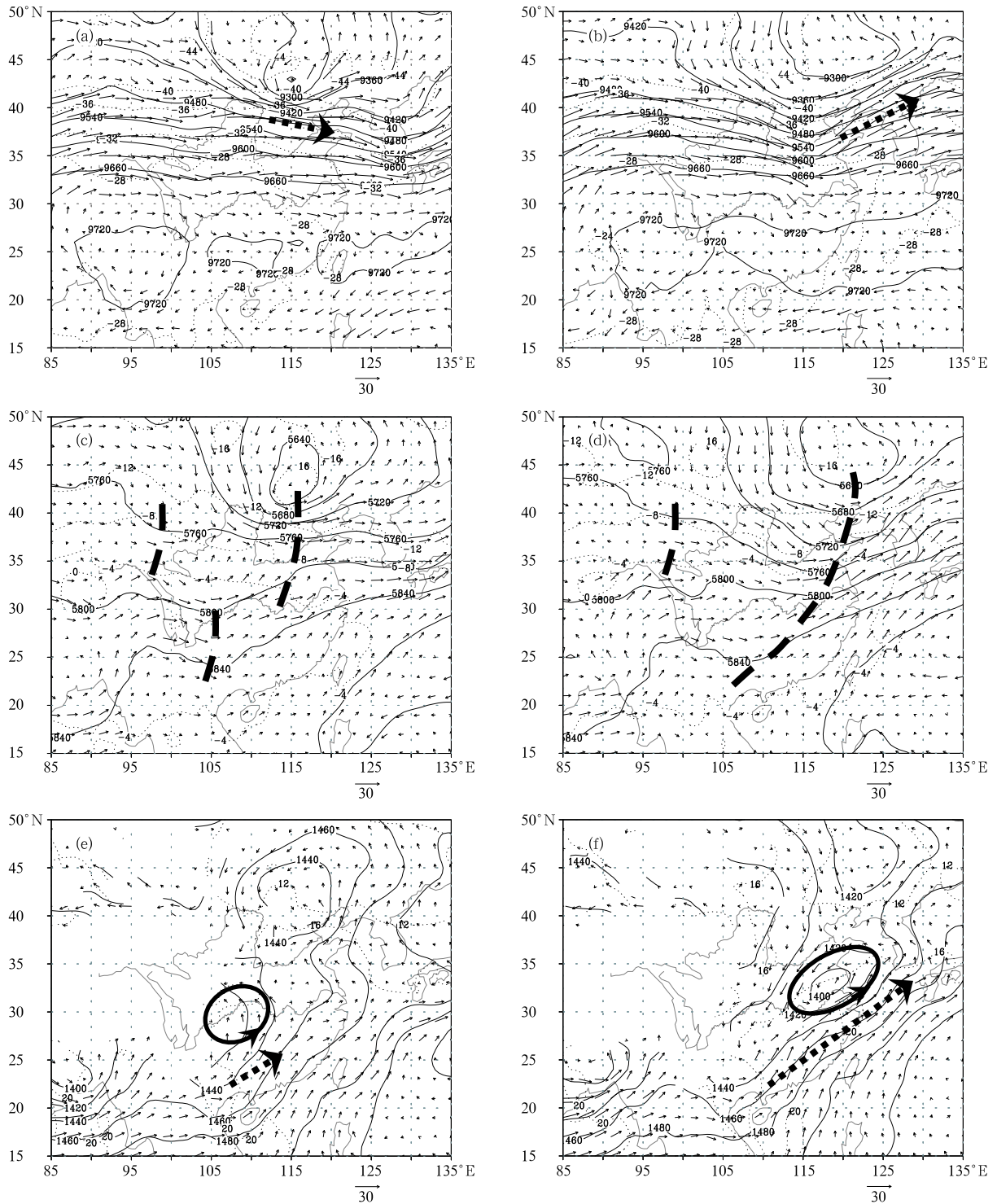


Fig. 3. Distributions of geopotential height (solid), temperature (dashed), and horizontal wind vectors at 300 hPa (a, b), 500 hPa (c, d), and 850 hPa (e, f) from the NCEP operational analysis at 0000 UTC 22 (a, c, e) and 0000 UTC 23 (b, d, f) June 1999. The bold dotted line in (a) and (b) indicates the ULJ streak. The bold dashed line in (c) and (d) indicates the upper-level trough. In (e) and (f) the bold dotted line indicates the LLJ and the bold solid circle indicates the low-level vortex.

low-level deformation and conduced increase of positive vorticity. At the same time, an LLJ developed over southern China, with an mLLJ over the south of the YHRB.

The evolution of the synoptic situation produced favorable conditions for Meiyu frontogenesis. The Meiyu front became mature during this 24-h period. At 0000 UTC 22 June, a 1000-km long band of a large equivalent potential temperature gradient and high potential vorticity (PV) maintained over the upper reaches of the Yangtze River, and a local dry-cold region was located over the MLYR without any distinct frontal structure (Fig. 4a). By 0000 UTC 23 June, a southwest-northeast oriented, 2000-km long Meiyu front developed along the entire reaches of the Yangtze River (Fig. 4b), with its position and length identical to the cloud band on the satellite image at this time (Fig. 2i). Within the Meiyu front, the equivalent potential temperature gradient was over 8 K (100

km)⁻¹, and the PV was over 1.0 PVU (1 PVU = 10⁻⁶ K m² kg⁻¹ s⁻¹), with some embedded PV maxima.

From the aforementioned synoptic analysis, key features of this heavy rainfall event can be summarized as follows. The combination and deepening of upper-level troughs created a background favorable for the Meiyu frontogenesis. The Meiyu front developed into a band of high PV with some maximum centers at lower levels over the MLYR. Associated with the Meiyu frontogenesis, a series of MCSs developed with accompanying LLJ, ULJ, and LMVs along the Meiyu front.

3. Model description and evaluation

3.1 Model description

The three-dimensional, compressible, nonhydrostatic, and primitive equation model ARPS (Advanced Regional Prediction System) is used in this study.

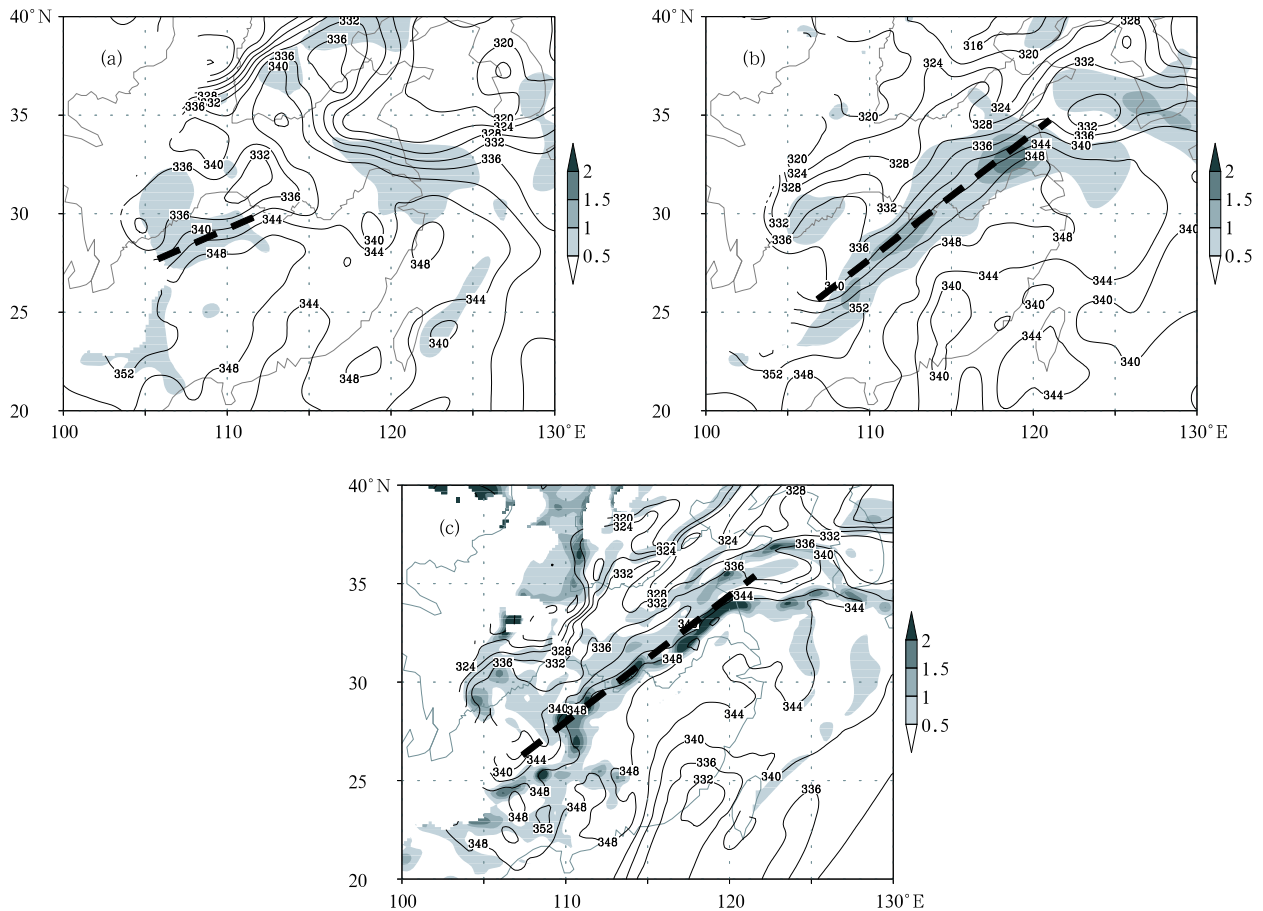


Fig. 4. The 850-hPa equivalent potential temperature (solid line, contour interval is 4 K) and potential vorticity (shaded; PVU) fields obtained from the NCEP operational analysis (a, b) and the ARPS model simulation (c) at 0000 UTC 22 June (a), and 0000 UTC 23 June (b, c). Bold dashed lines represent locations of the Meiyu front.

The model serves as an effective tool for basic and applied research, and as a system suitable for explicit prediction of convective storms as well as weather systems on other scales (Xue et al., 2000a, b). The model domain (Fig. 5) consists of two nested grids: a relatively coarse outer grid (D01, 45-km resolution, mesh size of 160×120) and a higher-resolution inner grid (D02, 15-km resolution, mesh size of 248×188). In the vertical, 32 terrain-following layers (the vertical resolution increases gradually from 20 m near the surface) with an averaged grid spacing of 625 m, are used for both grids over a depth of 20 km. This study will focus on the results over the inner domain.

All physical parameterizations are activated at both grids. The precipitation physics includes the modified mixed-phase microphysics scheme of Lin et al. (1983) for grid-scale convection, and the Kain-Fritsch cumulus parameterization scheme (Kain and Fritsch, 1993) for subgrid-scale convection. The 1.5 order TKE-based scheme (e.g., Deardorff, 1980) is used to parameterize the local mixing due to subgrid-scale turbulence. A detailed description of the ARPS model dynamics and physics can be found in Xue et al. (2000a, b).

The initial and lateral boundary conditions are obtained from the National Centers for Environmen-

tal Prediction (NCEP) global analysis data on a $1^\circ \times 1^\circ$ horizontal resolution. The initial fields from the NCEP analysis contain surface and radiosonde observations. The assimilation of observational data is done through an iterative interpolation scheme based on Bratseth (1986). The simulation is initialized at 0000 UTC 22 June 1999 and is concluded at 0000 UTC 23 June 1999. The lateral boundary conditions on the coarse mesh (D01) are updated at every time step by a temporal interpolation from the 6-h NCEP analysis, while the inner-mesh (D02) lateral boundary conditions are updated at each time step with the 1-h output from the outer mesh. The upper and lower boundaries are rigid, with a Rayleigh sponge layer above 14 km for both grids.

3.2 Validation of the numerical simulation

To establish confidence in the model diagnostics, an evaluation of the simulation results is offered here. As shown in Fig. 1b, the 24-h simulated rainfall valid at 0000 UTC 23 June 1999 exhibited a 2000-km long rain belt over the MLYR, with four distinct rainstorm centers, which are labeled with A' , B' , C' , and D' . Except that the intensity of the rainstorm C' was overpredicted, the other three rainstorms were well captured in both location and intensity by the model.

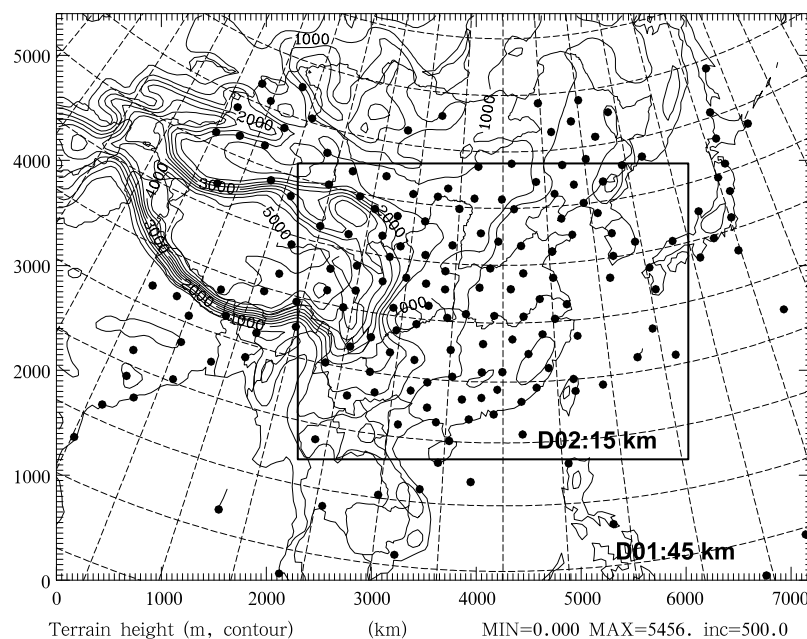


Fig. 5. Two nested model domains (D01, D02) and the model topography (contour intervals are 500 m). Bold dots mark locations of the sounding stations used in this study.

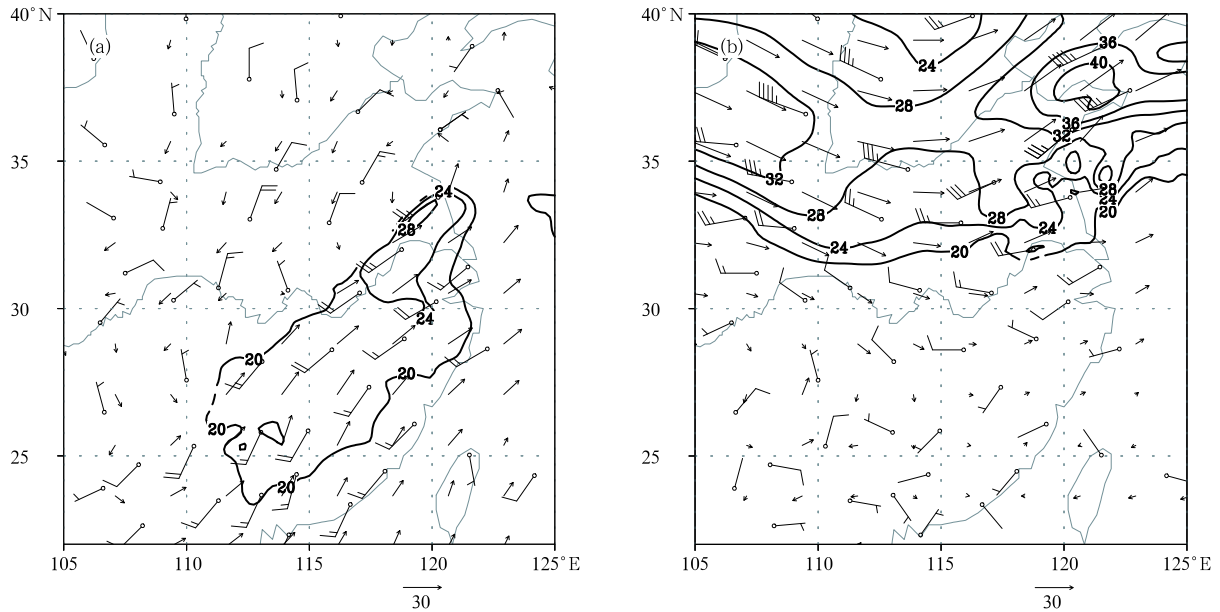


Fig. 6. Observed wind barbs and simulated wind vectors and isotaches exceeding 20 m s^{-1} (contour intervals are 4 m s^{-1}) at 850 hPa (a) and 300 hPa (b) at 0000 UTC 23 June. A full-barb wind flag corresponds to 10 m s^{-1} .

The location of the simulated Meiyu front at 0000 UTC 23 June 1999 was very close to that observed, and the distribution of positive PV maxima embedded in the front also resembled those of the observation (Fig. 4c). Moreover, some fine dynamical structures of the Meiyu front were obtained in the simulated results because of the high spatial resolution of the model. All available wind observations at 0000 UTC 23 June 1999 and the corresponding simulated wind fields were plotted in Fig. 6. Both the observed and simulated wind fields showed a cyclonic shear around the Meiyu front, with an LMV over the YHRB at 850 hPa. Also, the distribution and intensity of the simulated LLJ (with a maximum wind speed of about 28 m s^{-1}) and ULJ (maximum of about 42 m s^{-1}) were in decent agreement with those observed at low and upper levels. Based on the above validation, a detailed investigation on the scale interaction among the MWSs, and its impact on the development of MCSs along the Meiyu front, are carried out in following sections.

4. Model results: Evolution of the MWSs within the Meiyu front

4.1 Three-stage development of MCSs

During the warm season in East China, the MCSs

embedded in the Meiyu front are a main cause of heavy rainfall and are closely related to the LMVs (Chen et al., 1998, 2000). Regarding the interaction between the MCSs and LMVs in this particular case, the modeling results showed that it was rather complicated than the earlier view that the MCSs were triggered and strengthened entirely by an eastward moving SWV. In the present case, the evolution of the MCSs and LMVs could be divided into three different stages. To give a detailed description, the evolution of the 850-hPa streamline field and the composite radar reflectivity obtained from the model simulated hydrometeor concentrations are shown in Fig. 7.

The first stage was from 0000 to 0900 UTC 22 June (Figs. 7a, 7b, and 7c). During this period, the convections related to the MCSs were triggered and strengthened by an eastward-moving SWV, which is similar to the earlier view. As shown in Fig. 7a, at 0300 UTC 22 June, the SWV was located in the Sichuan Basin. The high reflectivity to its east indicated that convections were flared up over the region (Fig. 7a). In the next 3 h, the SWV moved eastward and its center was near 32°N , 108°E at 0600 UTC 22 June (Fig. 7b). An MCS near 30.5°N , 114.5°E , with a horizontal scale of over 100 km and the corresponding composite radar reflectivity exceeding 40 dBz, was observed. It was enhanced by southwesterly flows

associated with the SWV. By 0900 UTC 22 June, as the SWV moved eastward, a mesoscale convective band developed in the convergence region to the immediate south of the SWV (Fig. 7c). Moreover, to the southeast of the SWV, the convections of the MCS intensified significantly, following the rapid development of the lower-level cyclonic winds at the downstream region of the SWV.

The MCSs triggered and strengthened by the SWV acted to further increase the low-level positive vorticity and the cyclonic shear winds along the MLYR while they were propagating to the downstream region. However, the SWV moved more slowly than the MCSs. As a result, the SWV began to weaken and an LSL extending to the YHRB was established. The interaction between the MCSs and the LMVs entered into the second stage, which lasted from 1000 to 1700 UTC 22 June, and was characterized by the

formation of the LSL and further organization of the MCSs (Figs. 7d, 7e, and 7f). As the LSL strengthened and extended downstream, the MCSs over the MLYR propagated eastward along the LSL (Fig. 7d). By 1500 UTC 22 June, the MCSs developed further and were organized into a convective band by the LSL (Fig. 7e). It is interesting that some small LMVs were forming as the LSL got intensified. These small LMVs were correlated with the convections of the MCSs along the LSL, and they decayed rapidly when the convective centers moved downstream (Fig. 7f).

The third stage started at 1800 UTC 22 June and ended at 0000 UTC 23 June (Figs. 7g, 7h, and 7i). During this stage, an MCV formed over the YHRB mainly because of the latent heat release of the MCSs, and it had a strong positive interaction with the MCSs. As the MCSs were intensified, the cyclonic wind shear strengthened quickly over the YHRB. An MCV with

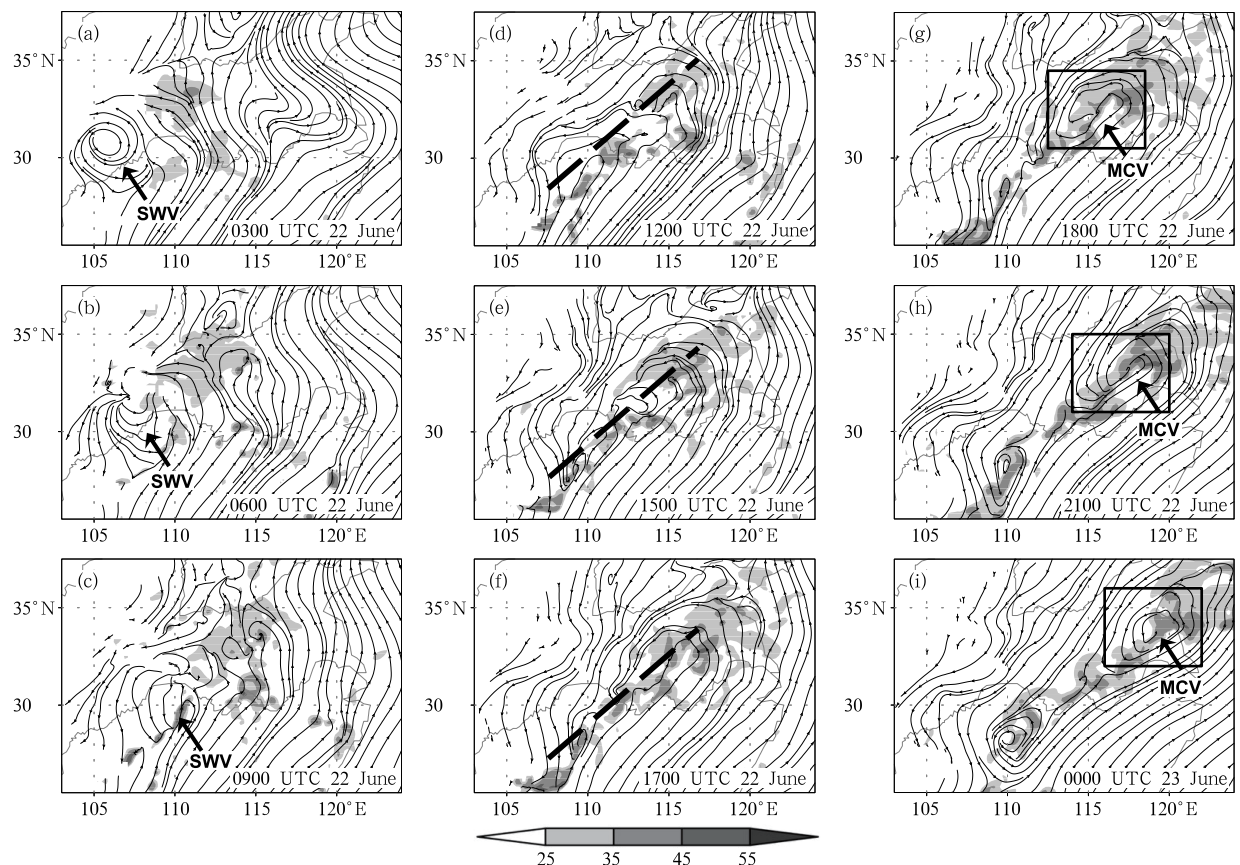


Fig. 7. The 850-hPa streamline field and the composite radar reflectivity (shaded; dBz) obtained from the model simulation results from 0300 UTC 22 to 0000 UTC 23 June 1999. The bold dashed line in (d), (e), and (f) indicates a line with strong directional shear and wind convergence, commonly referred to as LSL. The box in (g), (h), and (i) indicates the area selected for doing the averaging at the corresponding time in Figs. 10 and 11.

its center near 32°N, 116°E and at a horizontal scale of 300 km, formed at 1800 UTC 22 June (Fig. 7g). Accompanying the development of the MCV, the low-level convergence was promoted, which led to the further intensification of the MCSs. On the other hand, the strengthened MCSs induced stronger latent heat release, which led to further increase of low-level vorticity. This positive feedback between the MCSs and the MCV incurred a rapid intensification of the MCSs and the MCV in this period, similar to the nonlinear-CISK mechanism proposed by Cho and Chen (1995). By 2100 UTC 22 June, the horizontal scale of the MCV increased significantly as it moved eastward slowly, and the associated MCSs also grew quickly (Fig. 7h). By 0000 UTC 23 June, the MCV kept strengthening and moving eastward, and the MCSs were still in its mature stage, interacting strongly with the MCV (Fig. 7i).

From the above analysis, it can be seen that the MCSs responsible for the heavy rainfall were strongly correlated with the LMVs. The convection was firstly triggered by the SWV moving eastward, and developed into MCSs near the SWV. Then, an LSL formed after the SWV weakened. And then the MCSs were organized into a convective band along the LSL. Finally, an MCV developed at the northeast end of the LSL and had a strong positive feedback with the MCSs. In this three-stage evolution, the SWV, LSL, and MCV successively played their own vital roles in the development of the MCSs. This is a new dynamic mechanism for the interaction between the MCSs and the LMVs for this particular case. It has rarely been emphasized in earlier studies of Meiyu frontal heavy rainfall.

4.2 Three-stage evolution of LLJ and ULJ

Within the Meiyu front, the ULJ and LLJ on different scales usually play an important role in the development of MCSs during heavy rainfall events. In the present case, corresponding to the evolution of the MCSs and LMVs, the development of the ULJ and LLJ also experienced three different phases, and had significant correlations with the MCSs during each stage. Figure 8 shows the horizontal wind fields at 300 and 850 hPa in different phases. The areas with pre-

cipitation rate greater than 10 mm h⁻¹ are also plotted to depict the centers of the convection within the MCSs.

During the first stage (0000–0900 UTC 22 June), a ULJ streak (marked by U1) over North China, with a maximum wind speed of about 50 m s⁻¹, moved eastward together with a synoptic-scale low (Fig. 8a). Meanwhile, the west-southwesterly flow over the YHRB strengthened significantly, and became a part of the ULJ. It was notable that there were two apparent convection centers of the MCSs just behind the southern part of the ULJ. At lower levels, the southwesterly LLJ, with a wind speed of about 12–16 m s⁻¹, developed from South China to the MLYR as the SWV strengthened and moved eastward (Fig. 8b). A cluster of convections was located at the front edge of the LLJ. In the next 7 h (1000–1700 UTC 22 June), i.e., the second stage, the U1 moved northeastward quickly, and was too far north to affect the MCSs (Fig. 8c). However, a new ULJ streak (marked by U2) formed to the immediate north of the YHRB at 1500 UTC 22 June, which provided favorable upper-level divergence for the development of the MCSs over the YHRB. In this period, the LLJ further strengthened and extended northeastward (Fig. 8d). A local wind speed maximum (exceeding 16 m s⁻¹) appeared south of the MCSs at 1500 UTC 22 June. Such a horizontal wind disturbance was connected with a well-developed MCS. It is evident that the evolution of the LLJ and ULJ during this stage provided favorable conditions for the subsequent development of the MCSs. During the third stage (1800 UTC 22 June–0000 UTC 23 June), the primary feature of evolution of the ULJ and LLJ was the development of the mULJ and mLLJ. As shown in Fig. 8e, the U2 intensified and moved northeastward, with its right entrance quadrant to the immediate north of the YHRB. An mULJ, which firstly appeared at 2100 UTC 22 June, was evident to the east (downstream) of the MCS. At lower levels, as the LLJ strengthened, an mLLJ with a horizontal scale of about 300 km and a maximum wind speed of above 28 m s⁻¹, developed towards the south of the YHRB (Fig. 8f). It is suggested that the mULJ and mLLJ were results of the intense convections related to the

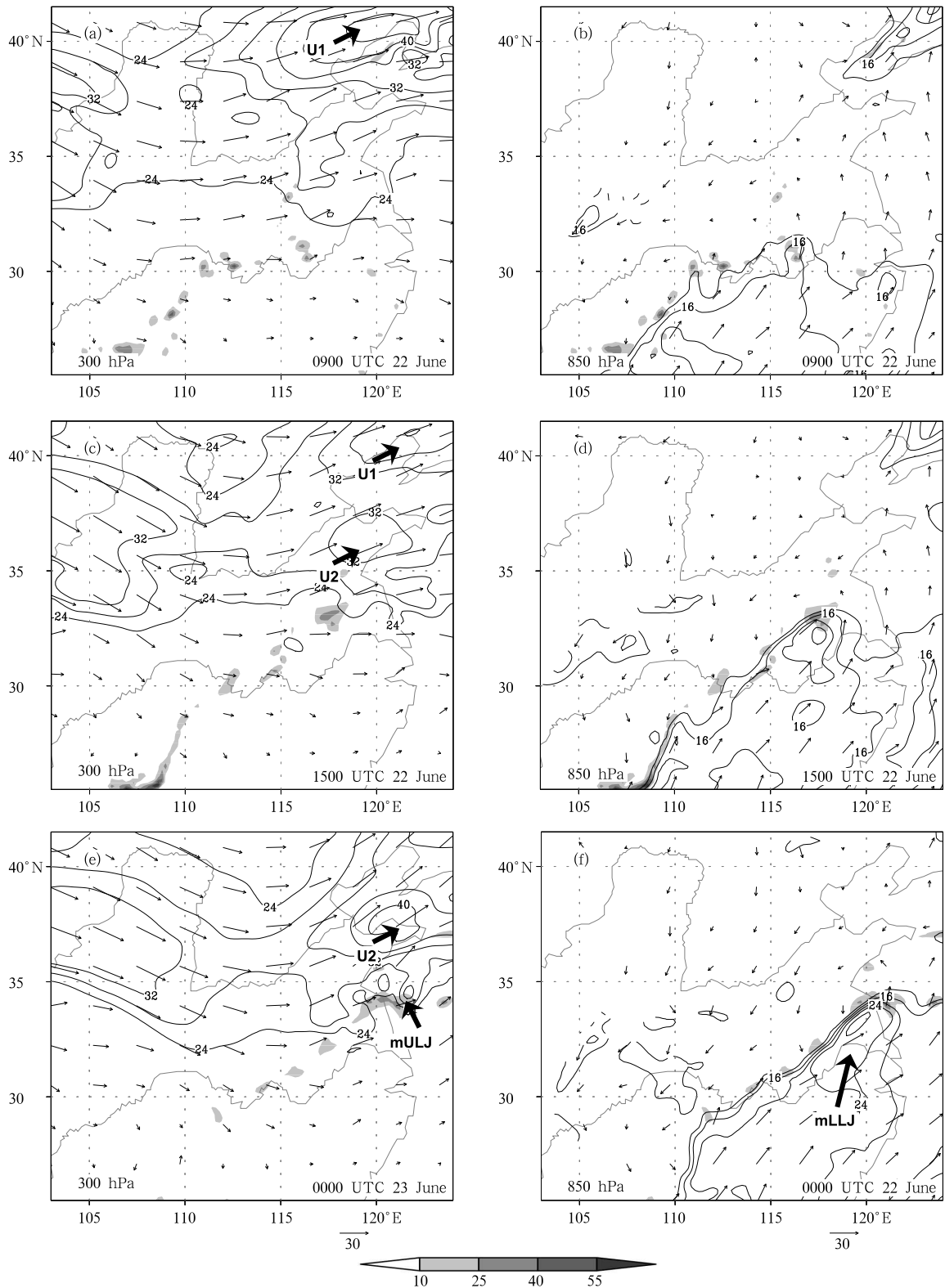


Fig. 8. Total precipitation rate (shaded; mm h⁻¹) and horizontal winds (vectors) at 300 hPa (left panels) and 850 hPa (right panels) at 0900 UTC 22 June (a, b), 1500 UTC 22 June (c, d), and 0000 UTC 23 June (e, f). The isotaches exceeding 12 m s⁻¹ at 850 hPa and 24 m s⁻¹ at 300 hPa are plotted with a contour interval of 4 m s⁻¹.

MCSs (Chen et al., 2000).

In view of the evolution of the MCSs and the LMVs, the three-stage evolution of the ULJ and LLJ indicated that the interaction among the MWSs gradually intensified and became a coupled development. Firstly, the ULJ streak (U1) led the LLJ to extend northeastward through the upper-level trough and the SWV moving eastward. Then, as the MCSs were organized by an LSL, the ULJ and LLJ was prompted, resulting in a new ULJ jet streak (U2) and the strengthened LLJ with a local wind disturbance. The new jet streak U2 and the local wind speed maximum in the LLJ provided a favorable environment for the MCSs. Eventually, mainly because of the positive feedback between the MCSs and MCV, the adjustment of wind related to the development of the MCSs induced the mLLJ, which fed stronger warm and moist air into the MCSs. A ventilated outflow in the upper troposphere was favorable for the formation of the mULJ that could further enhance the upper-level divergence and the updraft in the MCSs.

4.3 Vertical frontal circulations and the coupled development of MWSs

As analyzed in the previous sub-sections, the scale interaction within the Meiyu front experienced three different stages, and finally a coupled development of the MWSs at different levels was achieved. The MCSs, MCV, and LLJ were mainly located at low to middle levels, apart from the northern upper-level jet system. In this sub-section, it will be shown that the vertical frontal circulations played an important role in the coupled development of the MWSs.

Vertical cross-sections along 119.5°E are shown in Fig. 9. This plot illustrates the effect of the vertical frontal circulations at the second and third stage. The total water mixing ratio, i.e., the sum of mixing ratio of rain water, cloud water, cloud ice, snow, and hail, the equivalent potential temperature, and the horizontal wind speed are plotted to indicate the evolution of the MCSs, LLJ, ULJ, and the Meiyu front.

In Fig. 9, there are three main frontal vertical circulations: the updraft across the entrance of the ULJ streak, the cross-frontal circulation, and the inverse vertical circulation to the south of the Meiyu front. At 1500 UTC 22 June (Fig. 9a), the updraft across

the entrance of the ULJ streak exhibited a slantwise ascent from the lower level, which constituted a channel of momentum transport between low and upper levels. But the upward motion was rather weak (less than 0.01 m s^{-1}) at this time. The inverse vertical circulation was located at middle and upper levels in a warm sector, and had little effect on the low-level systems. The cross-frontal circulation was located at lower levels and its returning flow did not fully develop. As the MCSs developed (Fig. 9b), the updraft within the front was strengthened. The slantwise ascent changed to a strong perpendicular updraft, which was more intensely connected to the LLJ and ULJ through the enhanced vertical momentum transport. The inverse vertical circulation was also strengthened and extended to lower levels, and its increased returning flow further promoted the development of the LLJ. However, the cross-frontal circulation was not changed obviously at this time. When the MCSs became mature (Fig. 9c), the troposphere-deep, strong and perpendicular updraft further potentiated the interaction between the LLJ and ULJ, and the returning flow of the strengthened inverse vertical circulation accelerated the air parcel movement in the LLJ and mLLJ. The cross-frontal circulation developed well, and its returning flow encountered the mLLJ and strengthened the lower-level convergence. Through the Coriolis acceleration, the convergence flows enhanced the lower-level positive vorticity and prompted the development of the MCV. By 0000 UTC 23 June (Fig. 9d), although the updraft across the ULJ streak entrance was still strong, the inverse vertical circulation and the cross-frontal circulation weakened as the MCSs began to decay. It can be seen that through the adjustment of the vertical frontal circulations, the interaction among the MWSs was reinforced greatly. Evidently the vertical frontal circulation is a necessary condition for the scale interaction and the coupled development of the MWSs.

5. Model results: The interaction between MCV and MCSs

As shown in Section 4, in the third stage of the MCSs evolution, the MCV played a key role in the development of MCSs and formation of heavy rainfall.

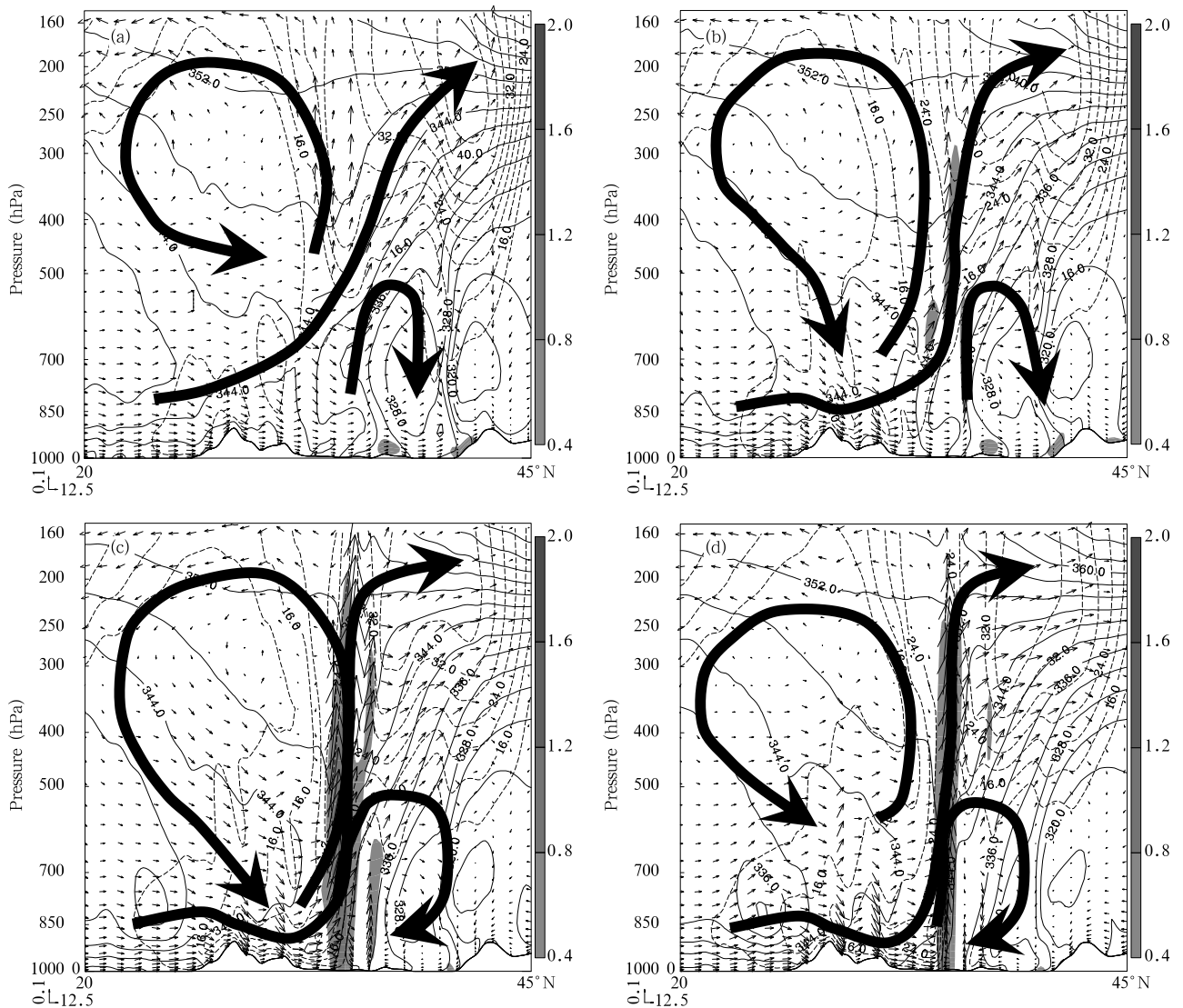


Fig. 9. Vertical cross-sections along 119.5°E (from 20° to 45°N) of the vertical circulations (vectors), total water mixing ratio (shaded; g kg^{-1}), equivalent potential temperature (solid; contour intervals are 4 K), and horizontal wind speed exceeding 12 m s^{-1} (dashed; contour intervals are 4 m s^{-1}) at (a) 1500 UTC 22 June, (b) 1800 UTC 22 June, (c) 2100 UTC 22 June, and (d) 0000 UTC 23 June. The bold arrows represent the vertical circulations within the Meiyu front.

The mechanism of the formation and development of such a MCV needs to be examined in detail. A PV diagnosis is conducted in this sub-section. The growth of PV implies local height fall and increase of cyclonic vorticity at lower levels (Hoskins et al., 1985), namely, the intensification of the MCV in the present case.

A time-height cross-section of area-averaged PV from 1500 UTC 22 to 0000 UTC 23 June is obtained to quantitatively describe the evolution of the MCV (Fig. 10a). The area for averaging is defined as a rectangular

region ($3^{\circ} \times 2^{\circ}$) centered at the MCV center, moving with the MCV when it propagated downstream (Figs. 7h and 7i). Note that before the formation of the MCV (1500 to 1800 UTC 22 June), the averaging area is fixed at the region in which the MCV appeared at 1800 UTC 22 June (shown in Fig. 7g). The corresponding time-height cross-section of area-averaged latent heat release, which signifies the evolution of the associated convective clusters, is also plotted to illustrate the temporal relationship between the MCV

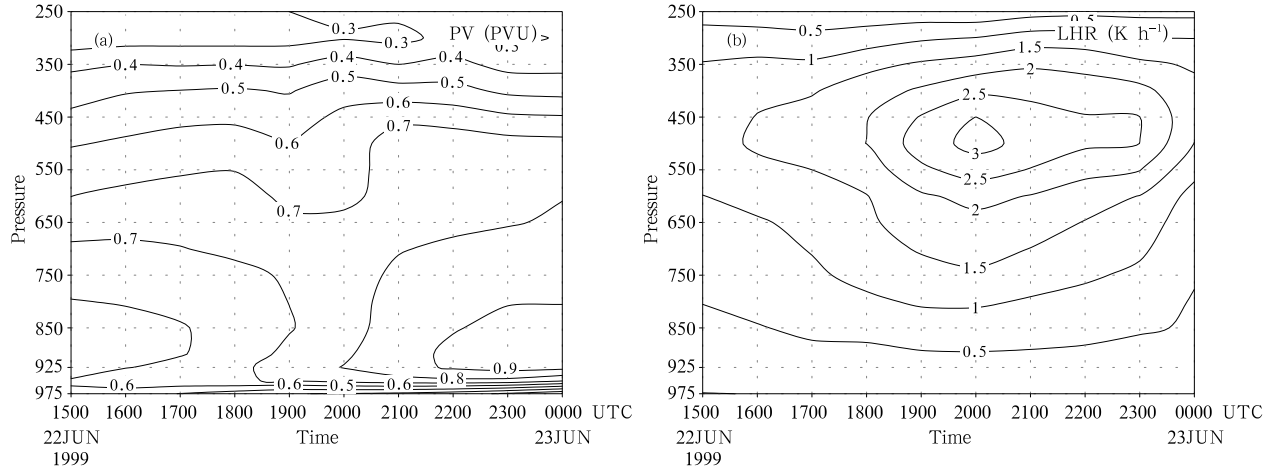


Fig. 10. Time-height cross-sections of area-averaged (a) potential vorticity (PV) (contour intervals are 0.1 PVU) and (b) latent heat release (contour intervals are 0.5 K h⁻¹) in the MCV developing region (the averaging areas are indicated in Figs. 7g-i).

and the MCSs (Fig. 10b). The latent heat release is calculated based on the temperature tendency terms derived from the cloud microphysics and cumulus parameterization related model outputs.

As shown in Fig. 10a, the low-level PV (below 700 hPa) was always increasing in this period, which was about 0.5 PVU at 1500 UTC 22 June and 0.98 PVU at 0000 UTC 23 June (Fig. 10a). This indicates the formation and continuous intensification of the MCV. The maximum low-level PV appeared after 2200 UTC 22 June, while at 2000 UTC 22 June the low-level PV reached the largest growth rate (about 0.08 PVU h⁻¹). However, the increment of mid- and upper-level PV (above 700 hPa) was very small in this period. From Fig. 10b, we can see that the averaged latent heat release at middle levels strengthened and extended to the lower levels from 1500 to 2000 UTC 22 June, and weakened gradually within the next 4 h (Fig. 10b). The maximum latent heat release appeared at middle levels (near 500 hPa) at 2000 UTC 22 June. By comparing Fig. 10a with 10b, it is evident that the MCV generation coincided with the outbreak of deep convections over the region, and the MCV developed most effectively when the MCSs were the strongest. However, when the MCSs began decaying, the MCV continued to intensify after 2000 UTC 22 June. This is similar to the Meiyu frontogenesis under the nonlinear-CISK mechanism (Cho and Chen,

1995).

To know more about the MCV development, the factors affecting the variation of area-averaged PV are examined using the Ertel's PV tendency equation, written as

$$\frac{\partial q}{\partial t} = -\mathbf{V}_h \cdot \nabla_h q - w \frac{\partial q}{\partial z} + \frac{1}{\rho} \left[\zeta_a \cdot \nabla \left(\frac{d\theta}{dt} \right) + \nabla \theta \cdot \nabla \times \mathbf{F} \right], \quad (1)$$

and the Ertel's PV is defined as

$$q = \frac{1}{\rho} \zeta_a \cdot \nabla \theta, \quad (2)$$

where $\zeta_a = f\mathbf{k} + \nabla \times \mathbf{V}$ is the three-dimensional absolute vorticity; ρ is air density; \mathbf{V}_h is horizontal wind vector and w is vertical component of wind, and \mathbf{F} is friction. The four terms on the right-hand side of Eq. (1) represent, respectively, the horizontal and vertical advection of q (referred to as HADV and VADV), the effect on q of diabatic heating/cooling that is almost entirely resulted from latent heat release in this case (referred to as LSRC), and the effect on q of friction (referred to as FSRC).

The time-height cross-sections of these four terms are interpolated to isobar surface and shown in Fig. 11 in comparison with Fig. 10. The LSRC was the most important factor responsible for the development of the MCV. The low-level positive LSRC

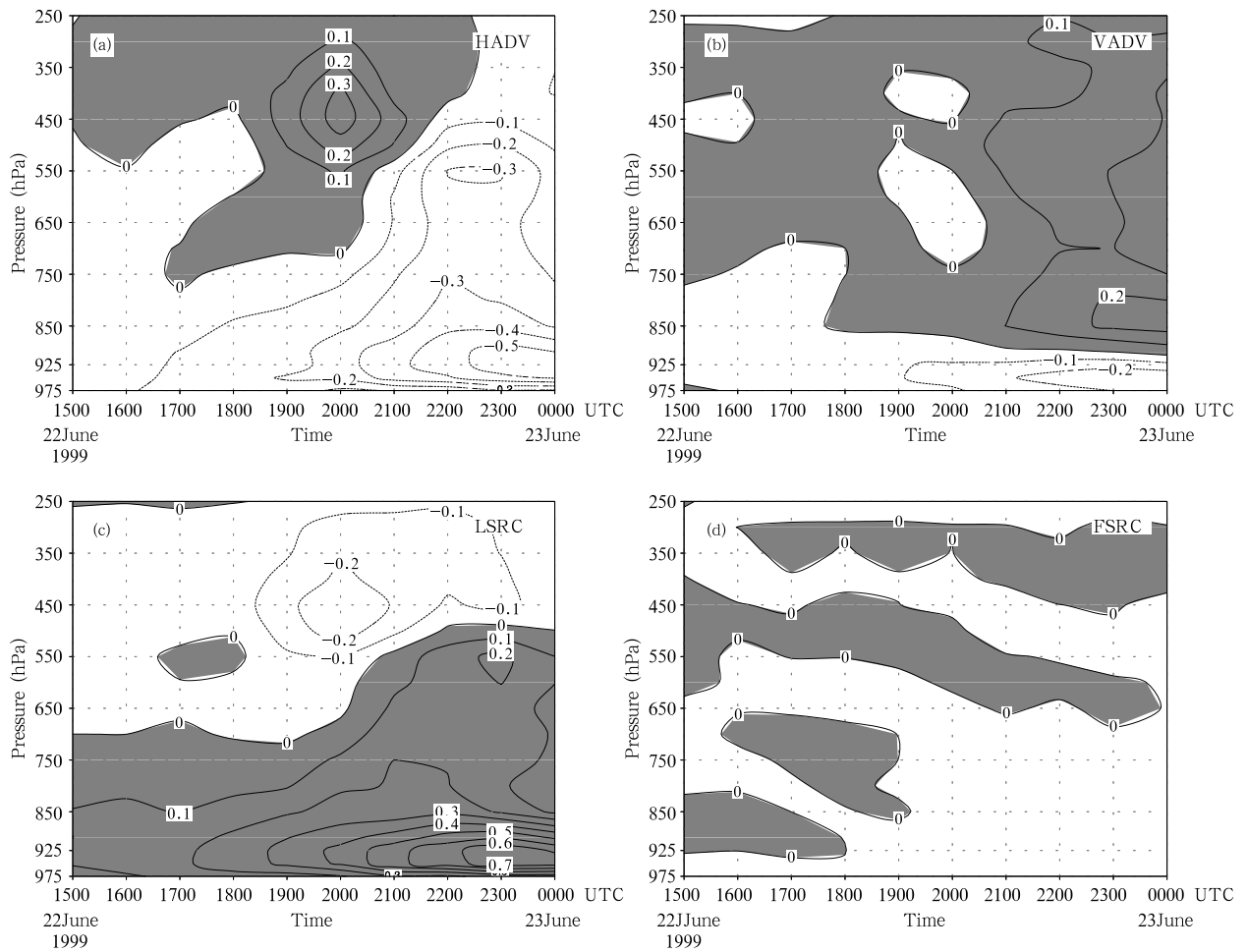


Fig. 11. As in Fig. 10, but for the effects of (a) horizontal advection, (b) vertical advection, (c) latent heat release, and (d) friction on potential vorticity (PV) of the MCV. Contour intervals are 0.1 PVU h^{-1} , and positive values are shaded.

was strengthening with time, and a relative weaker negative LSRC appeared at middle and upper levels (Fig. 11c). It implies that active cumulus convection could drastically enhance the low-level PV, leading to the formation and intensification of the MCV. The upper-level PV was destroyed by the latent heat release, which partially explains why the cyclonic circulation of the MCV was not able to extend to upper levels. The HADV had a nearly negative phase relationship with LSRC (Fig. 11a). Further analysis revealed that the low-level negative HADV was largely caused by the low-level PV flow that accelerated into the MCV. The negative VADV at low levels became significant after 1900 UTC 22 June, suggesting that the low-level PV was transported upward and had a negative contribution to the development of the MCV

(Fig. 11b). But its effect was smaller compared with the LSRC. The FSRC had little effect on the MCV in this case (Fig. 11d). Therefore, the MCV, which strongly prompted the MCSs, was a result of the latent heat release of the MCSs. The positive feedback between the MCSs and MCV led to their rapid development, strengthened subsequently the vertical frontal circulations, and enhanced the scale interaction among the MWSs.

6. Conclusions and discussion

This study provides evidence that heavy rainfall was produced by the scale interaction among the MWSs within the Meiyu front, including the SWV, MCSs, LMVs, MCV, (m)ULJ, and (m)LLJ. Although

the importance of the scale interaction among the MWSs within the Meiyu front was noted in previous studies, the particular physical process was not ever diagnosed and analyzed so far. The present study sheds light on how the scale interaction gears and impacts on the development of the MCSs within the Meiyu front. It is demonstrated that the scale interaction among different weather systems within the Meiyu front procured a coupled development for all the systems and caused heavy rainfall over the MLYR on 22 June 1999.

The three-stage evolution of the MCSs in this particular Meiyu heavy rainfall event can be described as following. During the first stage, the ULJ streak (U1) moved eastward together with a synoptic scale low, which strengthened the SWV at low levels. The LLJ developed simultaneously to the south of the SWV. Some convection were triggered and organized into MCSs by the SWV. During the second stage, although the SWV had decayed, the LSL was established, which strengthened and organized the MCSs along the Meiyu front. The MCSs development accelerated the LLJ and led to a new ULJ steak (U2). During the third stage, the latent heat release associated with the MCSs induced an MCV. An mLLJ subsequently developed to the immediate south of the convection band through a local mass-momentum adjustment during the development of the MCV. Much of the inflow into the MCSs was forced to go up to the upper troposphere, which accelerated the flow of air in the downstream region, and generated the mULJ. On the other hand, the local mesoscale structures including the MCV, mLLJ, and mULJ further prompted the MCSs.

The vertical frontal circulations possessed different structures and played a dynamic role at different stages. They reinforced the interaction among the MWSs within the Meiyu front. Adjusted by the MCSs, the updraft across the ULJ streak entrance, the cross-frontal circulation, and the inverse vertical circulation to the south of the Meiyu front were enhanced significantly, which strengthened the MWSs and their interaction at both upper and low levels. This resulted in the coupled development of the MWSs within the

Meiyu front.

A further PV diagnostic analysis for identifying the relation between the MCSs and the MCV showed that the MCV was generated and enhanced almost entirely by the latent heat release of the associated MCSs, and the MCV provided low-level convergence and helped organize the convection of the MCSs. This positive feedback process is a key characteristic of the scale interaction in this particular Meiyu heavy rainfall event.

Acknowledgments. The authors are grateful to Drs. K. K. Chu, Y. Zhang, and W. T. Wang for their assistance with the numerical modeling and simulation. The authors also thank the two anonymous reviewers for their precious comments.

REFERENCES

- Akiyama, T., 1973: The large-scale aspects of the characteristic features of Baiu front. *Pap. Meteor. Geophys.*, **24**, 157–188.
- Bratseth, A. M., 1986: Statistical interpolation by means of successive corrections. *Tellus*, **38A**, 439–447.
- Chen, G. T. -J., 1983: Observational aspects of Meiyu phenomena in subtropical China. *J. Meteor. Soc. Japan*. **61**, 306–312.
- Chen, G. T. -J., C. C. Wang, and S. C. -S. Liu, 2003: Potential vorticity diagnostics of a Mei-Yu front case. *Mon. Wea. Rev.*, **131**, 2680–2695.
- Chen, S. J., Y. H. Kuo, W. Wang, Z. Y. Tao, and B. Cui, 1998: A modeling case study of the heavy rainstorm along the Mei-Yu front. *Mon. Wea. Rev.*, **126**, 2330–2351.
- Chen, S. J., W. Wang, K. H. Lau, Q. H. Zhang, and Y. S. Chung, 2000: Mesoscale convective systems along the Meiyu front in a numerical model. *Meteor. Atmos. Phys.*, **75**, 149–160.
- Cho, H. R., and G. T.-J. Chen, 1995: Mei-yu frontogenesis. *J. Atmos. Sci.*, **52**, 2109–2120.
- Chu, K. -K., Z. -M. Tan, and M. Xue, 2007: Impact of 4DVAR assimilation of rainfall data on the simulation of mesoscale precipitation systems in a Mei-yu heavy rainfall event. *Adv. Atmos. Sci.*, **24**, 281–300.
- Deardorff, J. W., 1980: Stratocumulus-capped mixed layers derived from a three-dimensional model. *Bound.-Layer Meteor.*, **18**, 495–527.

- Ding, Y. H., 1992: Summer monsoon rainfalls in China. *J. Meteor. Soc. Japan*, **70**, 337–396.
- Gao Kun and Xu Yamei, 2001: A simulation study of mesovortices along Meiyu front during 22–30 June 1999. *Chinese J. Atmos. Sci.*, **25**, 740–756. (in Chinese)
- Hoskins, B. J., M. E. McIntyre, and A. W. Robertson, 1985: On the use and significance of isentropic potential vorticity maps. *Quart. J. Roy. Meteor. Soc.*, **111**, 877–946.
- Hu Bowei and Pan Efen, 1996: Two kinds of cyclonic disturbances and their accompanied heavy rain in the Yangtze River Valley during the Meiyu period. *Quart. J. Appl. Meteor.*, **7**, 138–144. (in Chinese)
- Kain, J. S., and J. M. Fritsch, 1993: Convective parameterization for mesoscale models: The Kain-Fritsch scheme. *The Representation of Cumulus Convection in Numerical Models. Meteor. Monogr.*, **46**, Amer. Meteor. Soc., 165–170.
- Kato, K., 1985: On the abrupt change in the structure of the Baiu front over the China continent in late May of 1979. *J. Meteor. Soc. Japan*, **63**, 20–35.
- Kuo, Y. -H., L. Cheng, and R. A. Anthes, 1986: Mesoscale analyses of Sichuan flood catastrophe, 11–15 July 1981. *Mon. Wea. Rev.*, **114**, 1984–2003.
- Kuo, Y. -H., L. Cheng, and J. W. Bao, 1988: Numerical simulation of the 1981 Sichuan flood. Part I: Evolution of a mesoscale southwest vortex. *Mon. Wea. Rev.*, **116**, 2481–2504.
- Liao Jie and Tan Zhemin, 2005: Numerical simulation of a heavy rainfall event along the Meiyu front: Influences of different scale weather systems. *Acta Meteor. Sinica*, **63**, 771–789. (in Chinese)
- Lin, Y. L., R. D. Farley, and H. D. Orville, 1983: Bulk parameterization of the snow field in a cloud model. *J. Appl. Meteor.*, **22**, 1065–1092.
- Xue, M., K. K. Droegemeier, and V. Wong, 2000a: The Advanced Regional Prediction System (ARPS)—A multiscale nonhydrostatic atmospheric simulation and prediction tool. Part I: Model dynamics and verification. *Meteor. Atmos. Physics*, **75**, 161–193.
- Xue, M., K. K. Droegemeier, and V. Wong., 2000b: The Advanced Regional Prediction System (ARPS)—A multiscale nonhydrostatic atmospheric simulation and prediction tool. Part II: Model physics and applications. *Meteor. Atmos. Physics*, **76**, 143–165.
- Yang, M. -J., Ben J. -D. Jou, S. -C. Wang, J. -S. Hong, P. -L. Lin, J. -H. Teng, and H. -C. Lin, 2004: Ensemble prediction of rainfall during the 2000–2002 Mei-Yu seasons: Evaluation over the Taiwan area. *J. Geophys. Res.*, **109**, D18203. doi:10.1029/2003JD004368.